2. TWO-ZONE MODEL FOR OBSERVED TEMPERATURE STRUCTURE

At each position along the spectrograph slit, the line of sight will cross several zones with different physical conditions. These may include:

A1: The compressed shell behind the bow-shock, which is in photoionization equilibrium;

A2: The main body of the jet bullet, also in photoionization equilibrium;

B1: The immediate post-shock cooling zone of the bow shock;

B2: The post-shock cooling zone of the jet shock.

In HH 204, the relative velocity between the unshocked jet and the working surface is very low ($\approx 15\,\mathrm{km\,s^{-1}}$), so the jet shock is much weaker than the bow shock, implying that the emission from zone B2 can be neglected compared with B1. Zones A1 and A2 should have similar conditions, and so can be merged into a single zone with density n_A and temperature T_A. Although the zone B1 should have a range of temperatures, for simplicity we assume a single characteristic temperature T_B. The density of zone B is found by assuming pressure equilibrium with zone A: $n_\mathrm{B} = n_\mathrm{A} T_\mathrm{A}/T_\mathrm{B}$. We define f_B for a given ion as the fraction of the total ionic emission measure, $\int n_\mathrm{e}\, n_\mathrm{ion}\, dz$, that comes from zone B, with the remainder, $f_\mathrm{A} = 1 - f_\mathrm{B}$, coming from zone A.

The appropriate value of T_B is rather uncertain, since it depends on the non-equilibrium evolution of ionization and temperature in the post-shock radiative relaxation layer. Most published shock models (Cox & Raymond 1985; Sutherland & Dopita 2017) are calculated on the assumption that the far upstream and downstream ionization states are determined by the radiation from the shock itself. Care must therefore be exercised when translating their results to cases such as HH 204, where external irradiation from O stars is a dominant factor. The curved bow shock in HH 204 should give a range of shock velocities, up to a maximum of $V \approx 84\,\mathrm{km\,s^{-1}}$ (assuming the pre-shock medium is stationary). In principle, this corresponds to post-shock temperatures as high as $2 \times 10^5\,\mathrm{K}$, but the gas at such temperatures will be too highly ionized to significantly emit optical lines. The cooling timescale is generally shorter than the recombination timescale, so the gas is over-ionized as it cools. It is only when the temperature falls below about 50 000 K that the abundance of O^{++} becomes significant (e.g., Fig. 11 of Allen et al. 2008), allowing the emission of the optical [O III] lines. A similar situation is seen in middle-aged supernova remnants, such as the Cygnus Loop (Raymond et al. 2020).

We look for solutions where both T_A and T_B are constant along the slit, so that any spatial variation in the temperature diagnostics is driven primarily by variation in f_B. Although the density diagnostics do show a gradient with position, both T([O III]) and T([S III]) are relatively insensitive to density, so for simplicity we assume n_A is constant. We use the Python library PyNeb to calculate the per-zone emission coefficients, $j(T_\mathrm{A}, n_\mathrm{A})$ and $j(T_\mathrm{B}, n_\mathrm{B})$, for each emission line. For a given diagnostic line pair, 1 and 2, the ratio is calculated as

$$R_{12} = \frac{(1 - f_\mathrm{B})\, j_1(T_\mathrm{A}, n_\mathrm{A}) + f_\mathrm{B}\, j_1(T_\mathrm{B}, n_\mathrm{B})}{(1 - f_\mathrm{B})\, j_2(T_\mathrm{A}, n_\mathrm{A}) + f_\mathrm{B}\, j_2(T_\mathrm{B}, n_\mathrm{B})}. \quad (2)$$

This is then fed into PyNeb's `getTemDen` function to find the equivalent single-zone temperature that would give the same ratio (assuming a density of n_A). It is clear from equation (2) that for $f_\mathrm{B} = 0$ one must recover $T_\mathrm{e} = T_\mathrm{A}$ and that for $f_\mathrm{B} = 1$ one must recover $T_\mathrm{e} = T_\mathrm{B}$. But for intermediate values of f_B, the derived temperature will differ between ions because of variations in the temperature sensitivity of the diagnostic ratios.

We first investigate the case of a common f_B for all ions, but we find that this is unable to reproduce the observations. This is demonstrated in Figure 4a, which shows the relation between T_e([O III]) and T_e([S III]) for 4 different values of T_B between 15 000 and 50 000 K. We set $T_\mathrm{A} = 9000\,\mathrm{K}$ and $n_\mathrm{A} = 20\,000\,\mathrm{cm^{-3}}$ in all cases and f_B increases from left to right along each curve. The gray rectangle shows the observed range of temperatures along the spectrograph slit (Figure 6): T_e([O III]) shows a systematic decline from $\approx 17\,000\,\mathrm{K}$ near the bow shock to $\approx 12\,000\,\mathrm{K}$ further away, while T_e([S III]) is roughly constant at 9000 to 10 000 K, with no apparent correlation with T_e([O III]). The two-zone models with $T_\mathrm{B} \geq 30\,000\,\mathrm{K}$ all show T_e([O III]) > T_e([S III]) as f_B increases, but this is insufficient to explain the observations. For example, in order to achieve T_e([O III]) = 17 000 K the models predict T_e([S III]) > 11 000 K, which is significantly higher than observed.

In Figure 4b, we relax the assumption of a common f_B for all ions, showing separately the predicted values of T_e([N II]), T_e([S III]), and T_e([O III]) as a function of f_B, assuming $T_\mathrm{B} = 30\,000\,\mathrm{K}$. The ranges of observed values are shown by colored bands, blue for [O III] and orange for [N II] and [S III]. From the figure it is apparent that a decline from f_B([O III]) ≈ 0.1 at $x = 0$ to f_B([O III]) ≈ 0.02 for $x > 5\,\mathrm{mpc}$ is required to explain the T_e([O III]) profile, whereas f_B([S III])) < 0.01 and f_B([N II]) < 0.01 is required at all positions.

It is not surprising that f_B should vary between ions since the photoionization equilibrium ion fraction of O^{2+}

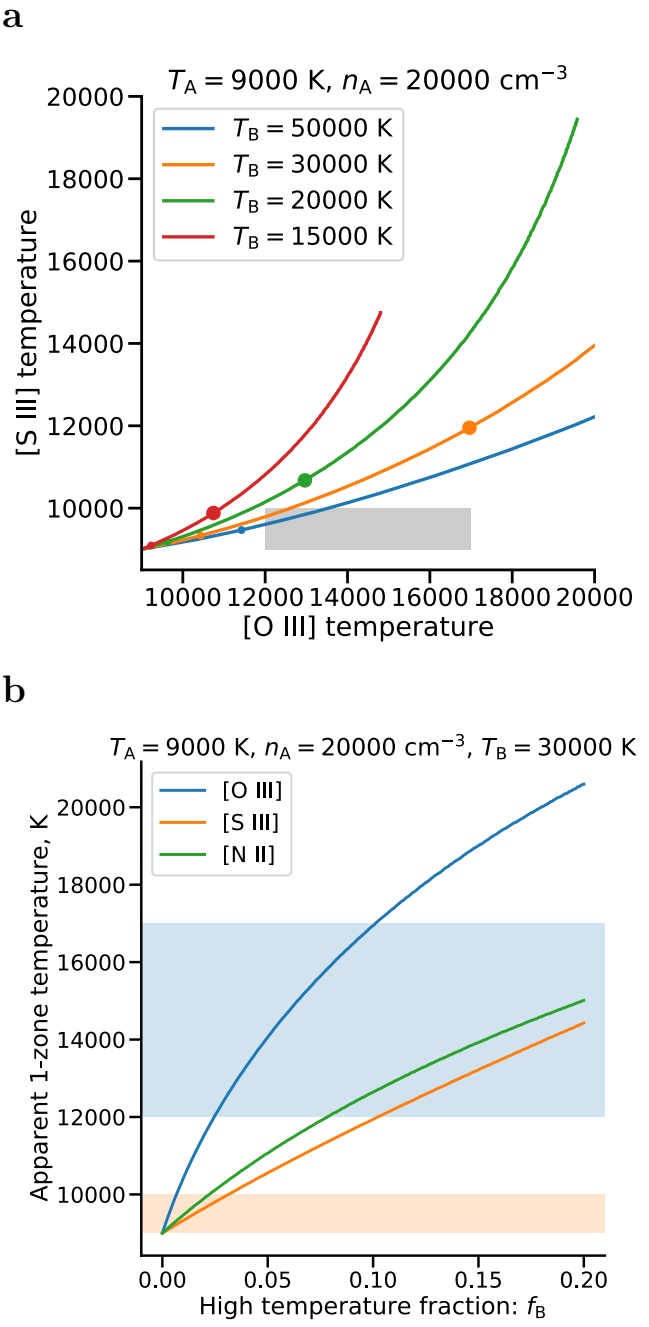

Figure 4. Simple two-zone model for spatial variations in temperature diagnostics. (a) Correlation between derived T_e from [O III] and [S III] lines, assuming that the fraction f_B of ionic emission measure that arises in the hot component (with temperature T_B) is the same for both ions. Values of $f_B = 0.01$ (small dots) and $f_B = 0.1$ (large dots) are indicated on each curve. The gray rectangle shows the observed range of values, which cannot be explained under this assumption (see text). (b) Derived T_e for [O III], [S III], and [N II] lines as a function of f_B, assuming $T_B = 30\,000$ K. Colored bands show the observed ranges, which imply that f_B([O III]) must be larger than for the other ions (see text).

from zone A is much lower than that of N^+ or S^{2+}. Assuming $f_B \ll 1$, then the ionic abundances given in the "Cut 1, HH 204" column of Table 4 correspond to zone A. These yield $O^{2+}/O = 0.005$ and $S^{2+}/S = 0.61$ if the abundances of unobserved ion stages are negligible. The lack of [N III] lines means that N^+/N cannot be estimated directly, but is likely of order unity. The fact that O^{2+} is only present in trace amounts in the photoionization equilibrium gas means that the relative contribution from the post-shock cooling zone is much larger than for S^{2+} and N^+. This is confirmed by emission line imaging of HH 204 (Weilbacher et al. 2015), which shows a morphology in [S III] and [N II] that is clearly dominated by the compact jet bullet, whereas the emission in [O III] is more diffuse within the parabolic envelope of the bow shock.

REFERENCES

Allen, M. G., Groves, B. A., Dopita, M. A., Sutherland, R. S., & Kewley, L. J. 2008, ApJS, 178, 20

Cox, D. P., & Raymond, J. C. 1985, ApJ, 298, 651

Doi, T., O'Dell, C. R., & Hartigan, P. 2002, AJ, 124, 445

—. 2004, AJ, 127, 3456

García-Díaz, M. T., Henney, W. J., López, J. A., & Doi, T. 2008, RMxAA, 44, 181

Kissler-Patig, M., Pirard, J. F., Casali, M., et al. 2008, A&A, 491, 941

Muench, A. A., Lada, E. A., Lada, C. J., & Alves, J. 2002, ApJ, 573, 366

O'Dell, C. R. 2009, PASP, 121, 428

O'Dell, C. R., & Doi, T. 2003, AJ, 125, 277

O'Dell, C. R., Ferland, G. J., Henney, W. J., et al. 2015, AJ, 150, 108

O'Dell, C. R., Hartigan, P., Lane, W. M., et al. 1997, AJ, 114, 730

O'Dell, C. R., & Wong, K. 1996, AJ, 111, 846

Raymond, J. C., Chilingarian, I. V., Blair, W. P., et al. 2020, ApJ, 894, 108

Rosado, M., de La Fuente, E., Arias, L., & Le Coarer, E. 2002, in Revista Mexicana de Astronomia y Astrofisica Conference Series, Vol. 13, Revista Mexicana de Astronomia y Astrofisica Conference Series, ed. W. J. Henney, W. Steffen, L. Binette, & A. Raga, 90–93

Sutherland, R. S., & Dopita, M. A. 2017, ApJS, 229, 34

Weilbacher, P. M., Monreal-Ibero, A., Kollatschny, W., et al. 2015, A&A, 582, A114